Turbulent Wake behind a Single Element Wing in Ground Effect

By

Xin Zhang and Jonathan Zerihan

Department of Aeronautics and Astronautics
School of Engineering Sciences
University of Southampton
Southampton SO17 1BJ
England
Tel.: +44 2380 594891
Fax: +44 2380 593058
Email: xzhang@soton.ac.uk

ABSTRACT

A study was performed in order to investigate the flowfield characteristics of a wing in ground effect. A highly cambered single element wing, with the suction surface nearest to the ground, was used to research the effect of changing the operating height from the ground at a single incidence. The results are of direct relevance to both aeronautical and racing car applications. A Laser Doppler Anemometry survey has been used to investigate the ground effect on the mean flow characteristics of the wake of the wing. The size of the wake was found to increase with proximity to the ground. A downward shift of the path of the wake was also observed. Instantaneous Particle Image Velocimetry elucidates the unsteady flow features. Discrete vortex shedding was seen to occur behind the finite trailing edge of the wing (Figure 1). As the ground height is reduced, separation occurs on the suction surface of the wing and the vortex shedding is coupled with a flapping motion of the wake in the transverse direction.

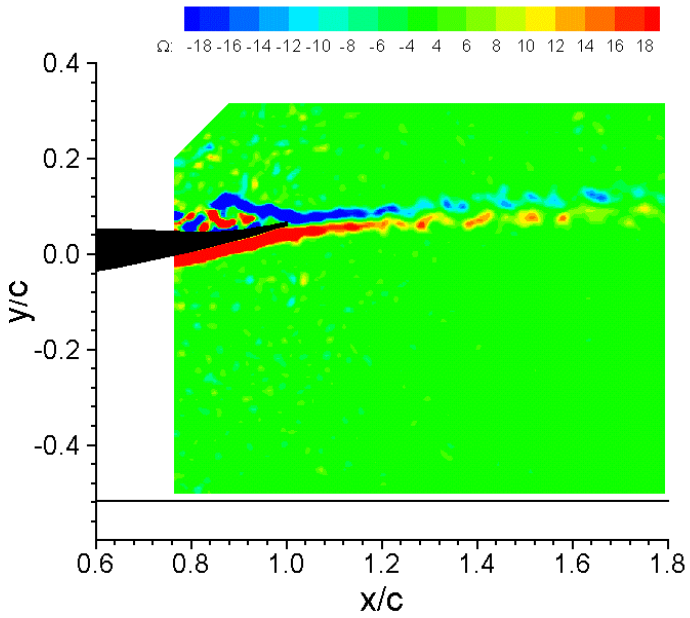

Fig. 1. Instantaneous vorticity contours behind wing with finite trailing edge

NOMENCLATURE

c	wing chord, 223.4mm
C_L	lift coefficient, $L/q_\infty S$. Positive lift implies a downforce; force directed to ground
h_r	ground height
Re	Reynolds number, $\rho U_\infty c/\mu$
U_∞	freestream velocity
u,v,w	velocity components in x,y,z axes system
uu, uv	turbulence quantities $\overline{u'u'}$, $\overline{u'v'}$
u_{min}	minimum component of u velocity component
x,y,z	Cartesian coordinates, x +ve downstream, y +ve up, z +ve to starboard
Greek Symbols	
α	incidence
δ	wake thickness, based on 99% thickness
δ_{bottom}	bottom of wake
δ_{top}	top of wake
μ	viscosity
ρ	density
ω	vorticity, $(\partial v/\partial x - \partial u/\partial y)c/U_\infty$
Glossary	
LDA	laser doppler anemometry
PIV	particle image velocimetry

1. INTRODUCTION

Wings in ground effect possess many aerodynamic features of both practical and fundamental interest. Recent research performed on the topic (Zerihan and Zhang, 2000) discusses the aerodynamic performance of a single element wing in ground effect, as applied to a racing car front wing. The downforce generated at different heights can be seen in Figure 2. The effect of the ground is to constrain the flow beneath the suction surface. At a large height in ground effect, the flow is accelerated over the suction surface to a greater level than in freestream, resulting in greater suctions on the suction surface. As the wing is brought closer to the ground, the flow is accelerated to a higher degree, causing an increased peak suction, and associated pressure recovery. At a height where the pressure recovery is sufficiently steep, boundary layer separation was observed at the trailing edge of the suction surface. As the height is reduced beyond this, the wing still generates more downforce, but the rate of increase slows, and the downforce reaches a maximum, the *downforce reduction phenomenon*. Below this height the downforce reduces. As the height is reduced from the first height

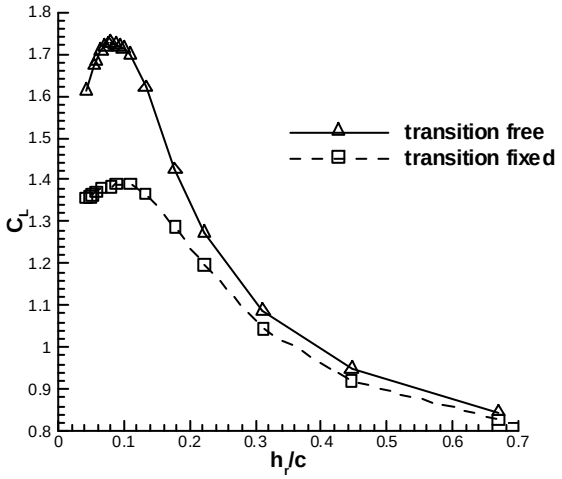

Fig. 2. Downforce in ground effect

at which flow separation was observed, the separation point moves forward steadily. At the maximum downforce, the boundary layer separates at approximately 80%c, for the free transition case. Heights greater than the maximum downforce are known as the force enhancement region. Below the maximum downforce is known as the force reduction region. Similarities can be drawn comparing the reduction of the height of a wing above the ground, with the increase of the incidence of a wing in freestream. In both cases, the pressure recovery becomes steeper, eventually causing boundary layer separation, and the wing stalls. The effect of fixing transition is to reduce the magnitude of the downforce, and to increase the height at which the force reduction phenomenon occurs.

As can be seen below in Figure 3, the wing has a finite trailing edge of 1.65mm thickness, corresponding to 0.007c. The existence of vortex shedding on wings with a finite trailing edge thickness has been well publicised, e.g. Pailhas *et al*. (1998), Vassilopoulos and Gai (1998), and Khorrami *et al*. (1999). Pailhas *et al*. (1998), have investigated a thick trailing edge aerofoil using LDA methods, and found the mean flowfield to be characterised by two counter-rotating vortices downstream of the trailing edge. Koss *et al*. (1993) obtained similar results. The authors compared the flowfield to the mean flow behind a Gurney flap; a twin vortex pair. High levels of normal stress $\overline{uu}$ were found, in two distinct peaks, in the near-field wake region. Jeffrey *et a.l* (2000) showed that the flowfield behind the Gurney was characterised by a wake of alternately shedding vortices. Recent work by Zhang and Zerihan, (2000) illustrates the vortex structure downstream of a Gurney flap fitted to a wing in ground effect.

Of contemporary interest is the wake generated from the wing. This effects the flow to the aerodynamic devices downstream, such as the underside and diffuser, the sidepods and cooling radiators, and the rear wing. The aerodynamic performance of the downstream devices may be adversely affected.

The current study forms part of a detailed investigation into wings in ground effect. The performance characteristics of a wing in ground effect have been presented in reference (Zerihan and Zhang, 2000). A multi-element configuration is currently being tested, and computational investigations using a RANS solver are underway. Results presented here are from LDA and PIV tests performed on the single element wing.

2. DESCRIPTION OF EXPERIMENT

2.1 Wind Tunnel

Experiments were performed in the University of Southampton 3.5m×2.5m R. J. Mitchell tunnel for the LDA and PIV surveys and the smaller 2.1m×1.7m wind tunnel for the other results. Both of the tunnels are of a conventional closed jet, closed circuit design. For correct modelling of the ground plane, the tunnels are equipped with a large, moving belt rig, with a layout similar to that described by Burgin *et al*. (1986). A system is located upstream of the belt for removal of the boundary layer that grows along the floor of the wind tunnel. The boundary layer is sucked away through a slot and a perforated plate. With the boundary layer suction applied, the velocity reaches the freestream value less than 2mm from the ground, corresponding to $h_r/c<0.01$. The freestream turbulence in the wind tunnels are less than 0.2%.

2.2 Wind Tunnel Model

The tests were performed on a single element rectangular wing, untapered and untwisted, of span 1100mm, and chord 223.4mm, corresponding to an aspect ratio of approximately 5. Endplates were used throughout testing, Figure 4. The wing profile was the main element of the Tyrrell 026 Formula 1 car front wing, Figure 3. Racing car designers originally used NASA GA(W) type wings. The current wing profile has evolved over a large period in time, from a GA(W) type wing.

The model was designed as an 80% scale model. Current wind tunnel testing of entire racing cars is performed using models not greater than 50% scale, at speeds of not more than 40m/s. The test speed of 30m/s and model size correspond to Reynolds numbers in the range approximately 20% to 50% higher than current racing car testing. The actual Reynolds number tested at, based on the chord of the wing, falls into the range of $0.430\text{-}0.462\times10^6$ due to fluctuations in ambient conditions. The tests were performed at constant velocity.

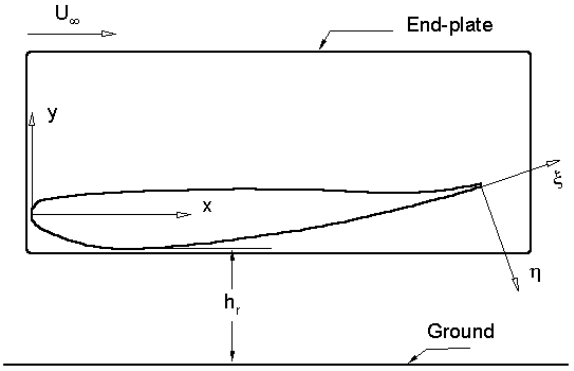

Fig. 3. Wing profile - Tyrrell-026 wing with endplate

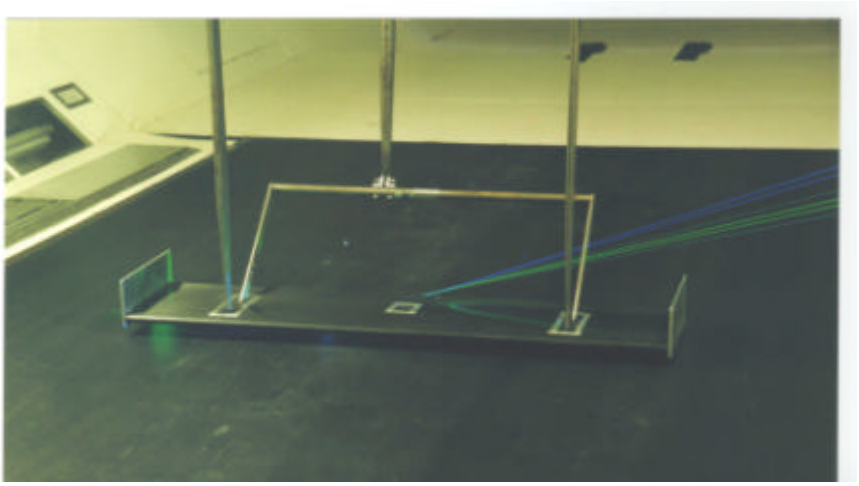

Fig. 4. Model installation in wind tunnel

All LDA and PIV tests were performed on a clean wing, without pressure tappings. Transition fixing was performed using strips of grit 1.3%c wide at 10%c from the leading edge on both surfaces, using 100 grit. In addition to the standard experimental reasons for fixing transition, the relatively low Reynolds number tested at generates a separation bubble over about 5% of the aerofoil chord for the free transition case, which would case problems for CFD modelling purposes. The results are also of fundamental interest as it is common for the wing to pick up dirt, dust, and debris throughout the race.

2.3 Experimental Procedures and Systems

Results for LDA and PIV tests presented here were performed for a range of heights in the force enhancement and force reduction regions; from $h_r/c=0.067$ to $h_r/c=0.448$. The height was defined by the distance from the ground to the lowest point on the wing, with the wing incidence set to zero deg, Figure 3. The incidence of the wing was then varied using a rotation about the quarter chord position. All quoted incidences are measured relative to a line at 2.45 deg to the chordline. Thus the 'true incidence' equals the quoted incidence plus 2.45 deg. The reference incidence of 1 deg is the incidence corresponding to endplates parallel to the ground, with the wing in its datum position as on the car.

Near-field LDA surveys were performed over an area from above the trailing edge to the ground plane, in the vertical direction, extending from the trailing edge to $x/c=1.2$ in the chordwise direction, with approximately 500 points in the grid. A fine grid spacing was used near to the trailing edge, and the ground. Far-field wake surveys were performed at three chordwise positions, corresponding to $x/c=1.5$, 2.0 and 3.0. The space between points was reduced both in the turbulent region from the wake

from the wing, and was reduced to a greater extent very close to the ground. Approximately 70 points were used in each wake survey. In addition to this, a selection of boundary layer surveys was performed on the suction surface at the trailing edge.

LDA measurements were performed with a three-component Dantec system with a 5W Ar-ion laser generator. The system was operated in backscatter mode. The velocities measured in the beam axes were resolved into the tunnel coordinate system *(x,y,z)* using a matrix transformation. Seeding was introduced by three seeding generators located downstream of the rolling road, behind the model. The LDA signals were analysed using three Dantec Burst Spectrum Analysers. On average, a total of 800 bursts (instantaneous samples) were collected for each data point.

In order to investigate any unsteady flow features, PIV was performed using a Dantec PowerFlow system. The laser for the PIV system was located approximately 1.5m downstream of the centre of the wing, after the end of the rolling road. The region of the flowfield including the trailing edge region, from the ground to above the wing, extending to $x/c \approx 1.8$ at the wing semi-span, was mapped. To perform this, a perspex endplate was used. In order to illustrate the flowfield phenomena of interest, results had to be processed on a very fine grid, the spacing between grid points corresponding to 1.48mm (0.0066c). This has lead to some noise in the results, especially where measurements were taken through the endplate. The analysis sequence used was to cross-correlate the data on 32×32 pixels, and perform a range validation of the resulting vectors, generating a 157×125 grid. No filtering was used as this was found to 'blur' the results significantly in regions of high velocity gradients. Although the instantaneous flow features are of primary interest from the PIV results, 50 snapshots were taken for most heights, to form a comparison with the LDA results, see below.

2.4 Errors and Uncertainties

The incidence of the wing was set to within ±0.005 deg, and the height above ground was set to within ±0.2mm. Belt-lifting was not observed under the flow conditions tested. The tunnel speed was run at a constant dynamic pressure of 56.25mm water ±0.05. Using procedures detailed by Moffat (1982), the errors in C_L were calculated using the addition method and a 95\% confidence; the worst case occurring at a height of 0.056c, and corresponding to a C_L of 1.678±0.009. Repeatability was found to be excellent.

Estimations of the 95% confidence interval in the LDA results using procedures given by Benedict and Gould (1996), are given in Figure 5. In this figure, wake profiles are presented at a height of $h_r/c=0.448$, for three chordwise locations. Typical values in the turbulent wake are ±0.0004 for the turbulence stresses $uu/U_¥^2$ and $uv/U_¥^2$. The further from the centre of the wake, the uncertainty typically decreases as the levels of turbulence reduce. The smoothness of the results suggests that the actual errors are significantly less than the quoted values for the uncertainty.

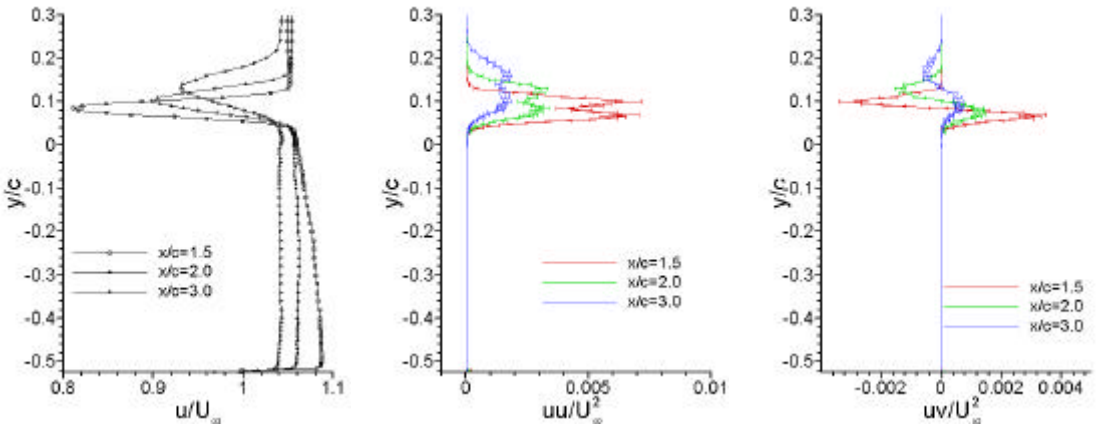

a) *b)* *c)*

Fig. 5. Mean flow wake profiles at $h_r/c=0.448$, (a) $u/U_¥$ (b) $uu/U_¥^2$ (c) $uv/U_¥^2$

Taking the mean of the PIV snapshots gives an indication of the quality of the data, when compared to the LDA results. In the Figure 6, results are compared for a height of $h_r/c=0.313$. The maximum velocity deficits in the wake are very similar, and outside the boundary layer, the velocities also agree well. There is a slight jaggedness to the PIV results outside the boundary layer. Although it is possible that this is because only 50 datasets were average, a similar effect was seen on a run performed with 500 flow snapshots. The likely explanation is the lack of filtering, and the noise generated when processing results at the very fine grid level for some of the snapshots.

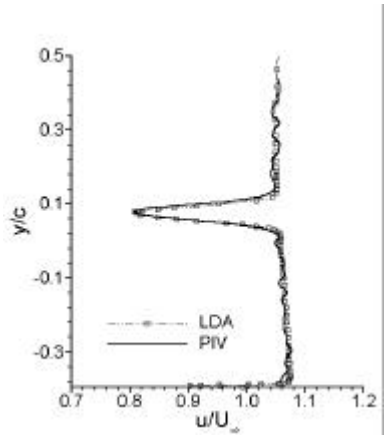

Fig. 6. Mean flow $u/U_{¥}$ velocity wake profiles as obtained from LDA and PIV systems, at $h_r/c=0.313$, $x/c=1.5$

3. RESULTS AND DISCUSSIONS

3.1 Aerodynamic Performance

The downforce generated at different heights from the ground can be seen in Figure 2 and is discussed in the introduction. As discussed above, the peak suction increases as the ground is approached, causing an increase in pressure recovery. This results in boundary layer separation, and a loss of downforce. Zerihan and Zhang (2000), discuss the topic in detail, and presents forces, surface pressures, and oil flow visualisation.

3.2 Off-surface flow measurements; Unsteady flow results

Figure 7 shows instantaneous vorticity contours at ride heights of $h_r/c=0.448,0.179,0.134$ and 0.067. The results represent a typical snapshot of the unsteady flow field.

At a ride height of $h_r/c=0.448$, the wake from both the pressure and the suction surface is characterised by areas of high and low vorticity concentrations, which suggest that discrete vortex shedding is occurring. At a height of $h_r/c=0.179$, the discrete vortex shedding can again be observed, although the structure of the vortices is different from that at $h_r/c=0.448$. The vortices emanating from the pressure surface are larger and stronger, and seem discrete. The vortices from the suction surface are again larger and stronger than for the case at the greater height. However, they seem less ordered. The separation between consecutive vortices has increased. At a height of $h_r/c=0.134$, all the vortices appear stronger, less regular, and more chaotic. Formation of the first vortex seems to be delayed, and for a short distance, the wake appears similar to an unstable shear layer experiencing a flapping motion in the transverse direction. At $h_r/c=0.067$, the change is amplified again, and the unstable shear layer lasts to $x/c»1.2$. More unsteady features are introduced to the vortices, and they are stronger than before.

The vorticity contours at the different heights are similar to results taken of the flow behind a Gurney flap on a wing in ground effect (see Zhang and Zerihan, 2000). As the boundary layer on the suction surface thickens, due to increasing ground proximity, the vortices become larger. The alternate vortex shedding was found to breakdown in close proximity to the ground, with the separation of the suction surface boundary layer. The wake experiences a flapping motion in the transverse direction.

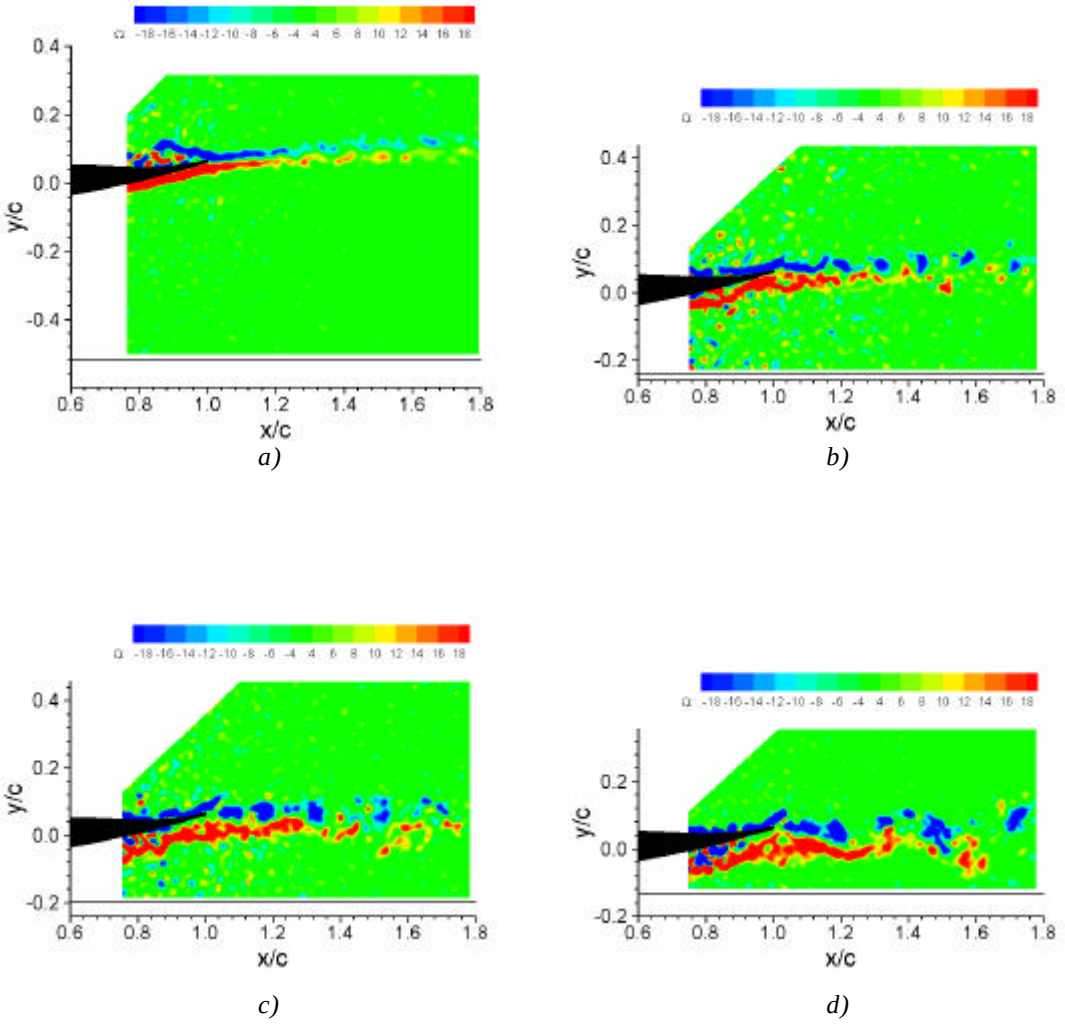

Fig. 7. Instantaneous vorticity contours a) $h_r/c=0.448$, b) $h_r/c=0.179$, c) $h_r/c=0.134$, d) $h_r/c=0.067$

The current results highlight the existence of vortex shedding behind a wing with a finite trailing edge. It is difficult to estimate the discrete frequency of the vortex shedding. Results behind the Gurney (Zhang and Zerihan, 2000) yielded a discrete frequency for the shedding. Of significance regarding vortex shedding is the thickness of the separating shear layers with respect to the distance between the shear layers. From LDA results, the time-averaged thickness of the boundary layer at the trailing edge of the suction surface was found to be approximately *0.05c* for a typical height in the force enhancement region, see Figure 9. The thickness of the finite trailing edge is 0.007c. The height of the Gurney gives a distance of 0.029c between the shear layers at the trailing edge. The thickness of the boundary layer at the trailing edge (of the suction surface) will vary with time because of its turbulent nature. The range of the ratios of the boundary layer thickness to the distance between the shear layers will be larger for the clean wing, than for the wing with the Gurney flap. This implies that the vortex shedding for the clean wing with the finite trailing edge will be less regular than for the wing with the Gurney, in terms of the discrete frequency at which the vortices are shed. Indeed, Vassilopoulos and Gai (1998), found that a turbulent boundary layer which increased the shear layer instability had the effect of increasing the number of discrete shedding frequencies.

3.3 Mean flow results

Figure 8 presents time-averaged LDA results for the u/U_{∞} velocity contours for the wing in ground effect at heights of $h_r/c=0.448$, *0.224, 0.134* and *0.067*. The general flow features of interest can be

seen qualitatively in the plots. The wake becomes thicker as is moves downstream, with the velocity deficit reducing due to small-scale turbulence. As the ground is approached, the wake increases in size, and velocity deficits become larger. In addition to this, the path of the wake changes, such that the angle reduces with increasing ground proximity. Between the wake and the ground, the flow faces an adverse pressure gradient, especially visible in the region of *x/c=1.0-1.5*. For the lowest case to the ground, $h_r/c=0.067$, the wake from the wing merges with the ground plane, at *x/c»1.5*. This is a height below the force reduction phenomenon.

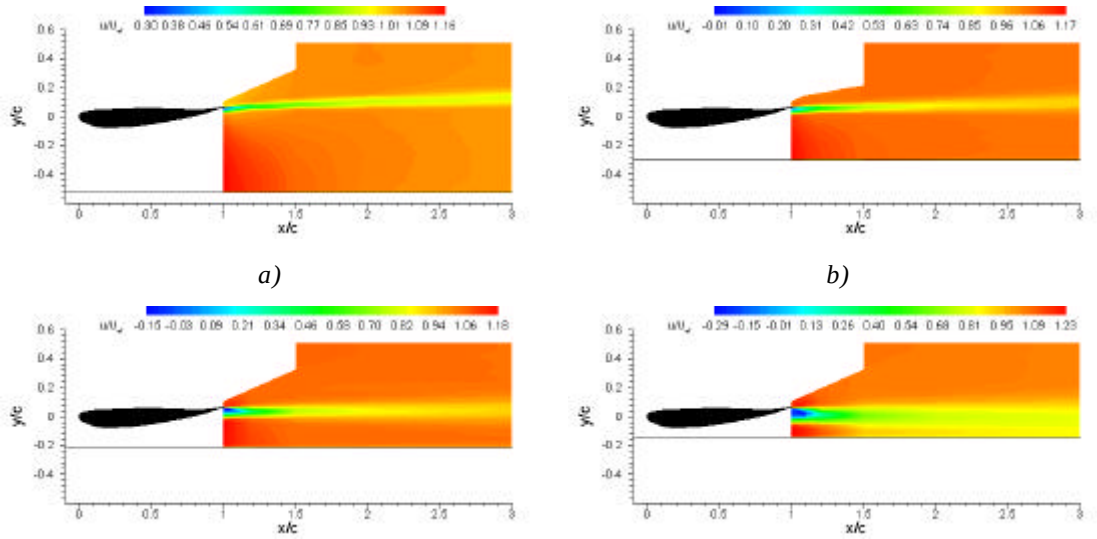

Fig. 8. Mean $u/U_¥$ velocity contours (a) $h_r/c=0.448$, (b) $h_r/c=0.224$, (c) $h_r/c=0.134$, (d) $h_r/c=0.067$

Boundary layer profiles taken on the suction surface at the trailing edge of the wing, Figure 9, illustrate the thickening of the boundary layer as the ground height is reduced, causing the increase in peak suction and associated adverse pressure gradient. For the $h_r/c=0.224$ case, the boundary layer seems very close to separation. The results at the two lower heights clearly show separation.

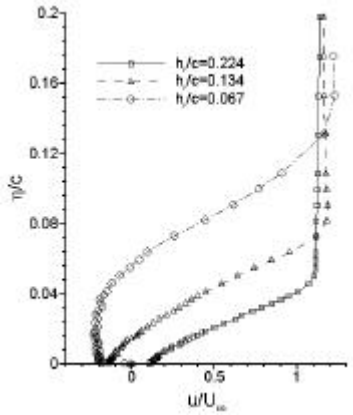

Fig. 9. Mean flow $u/U_¥$ velocity boundary layer profiles, taken at trailing edge on suction surface.

Figure 10a shows a series of wake surveys performed at a height of $h_r/c=0.224$, a typical height in the force enhancement region. For clarity, the symbols represent only every other data point. Small scale turbulence can be seen to diffuse the wake as it moves downstream. The velocity at the maximum velocity deficit increases from $u/U_¥=0.79$ at *x/c=1.5* to *0.88* at *2.0* and *0.93* at *3.0*. The height at which this occurs increases from *y/c=0.06* to *0.08* and *0.11*, for the three locations, as the height of the wake increases, as can be seen in the contours, Figure 8. The height at the top of the wake, as defined by the 99% velocity at the edge of the wake, increases from *y/c=0.12* to *0.15* and *0.19* at the three locations. This compares with the height at the bottom of the wake remaining approximately constant

at *y/c=0.01, 0.01 and 0.00* respectively. The thickness of the wake increases from d*=0.11* to *0.14* and *0.19*. Information regarding the growth of the wake for several different heights has been tabulated in Table 1. Similar results for heights of h_r/c*=0.134* and *0.067* are presented in Figure 10, and in Figure 5a for h_r/c*=0.448*, giving similar trends as the wake moves downstream.

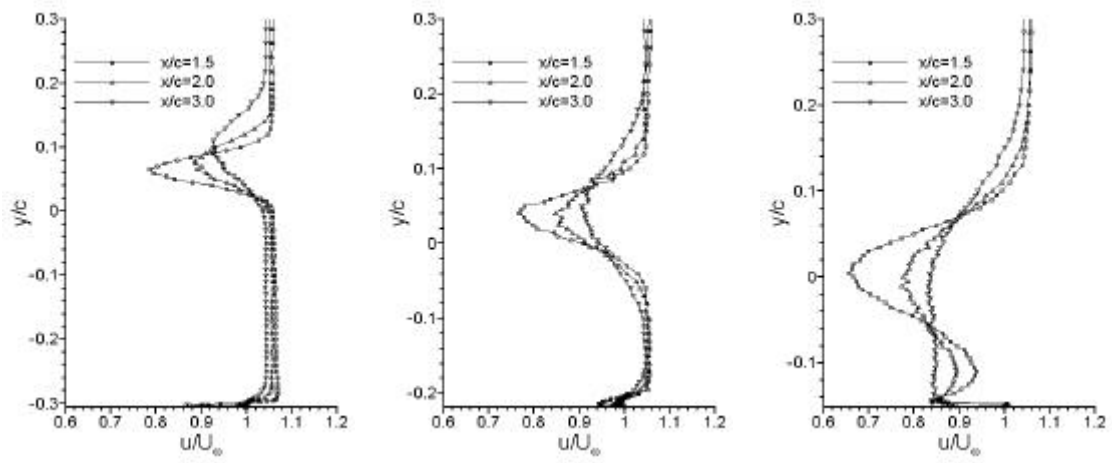

a) *b)* *c)*

Fig. 10. Mean flow u/U¥ velocity wake profiles, (a) h_r/c=0.224 (b) h_r/c=0.134 (b) h_r/c=0.067

The effect of changing the height of the wing above the ground on the wake at *x/c=1.5* is shown in Figure 11. The wake grows significantly as the ground is approached, from d*=0.09* to *0.11, 0.17*, and *0.23*. Again, these are available in Table 1. For the smallest height, h_r/c*=0.067*, the wake has merged with the ground, and the quoted size for the thickness is not strictly valid. For the next height, h_r/c*=0.090*, (not illustrated here) the wake appears close to merging with the ground. The location of the top of the wake remains constant, at *y/c»0.12*. However, the bottom reduces height from *y/c=0.04* for the greatest ride height to *-0.11* for the smallest height. This has the effect of lowering the height at which the maximum velocity deficit occurs as the ground is approached. The maximum velocity deficit also increases.

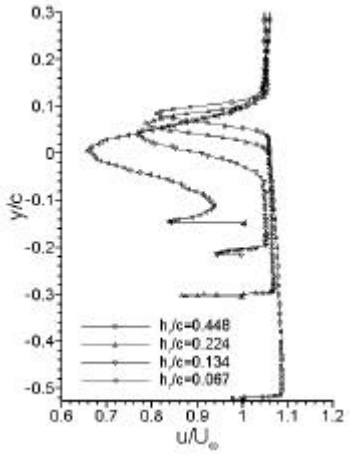

Fig. 11. Mean flow u/U¥ velocity wake profiles at x/c=1.5

As the ground height is reduced, the adverse pressure gradient increases, eventually leading to separation, as shown above. Hence, as the ground height is reduced, the boundary layer on the suction surface, and hence the wake from this will increase in size. It is this mechanism that causes the wake to grow as the ground is approached, due to the location of only the bottom of the wake changing, as can be seen in the results.

Very close to the ground, a deficit in velocity can be seen. This forms part of the ground flow, extending towards the values of constant velocity. The fact that the ground moves with velocity $u/U_{¥}=1.0$ implies that the region of velocity deficit is actually a separated flow region on the ground. For the practical case, the flow separating on the ground will tend to pick up dust and throw it up to the surrounding flow. Due to the very fine spacing between measurement points and steep velocity gradients, is it difficult to compare the velocity deficit part of the ground flow in terms of outright velocity. However, the thickness can be seen to increase with increasing ground proximity. It is believed that this is formed due to flow very close to the ground retarding, due to the adverse pressure gradient encountered from the point of maximum suction. As stated above, the adverse pressure gradient increases with ground proximity, which enforces this hypothesis. In fact, the flow exhibits features similar to a wall jet type flow.

Figure 12 shows profiles for the normal stress *uu* and primary shear stress *uv* from the wake surveys at $x/c=1.5$. As expected, the turbulent wake features high levels of *uu*. As the wake becomes larger, due to the smaller ground height, the perturbations become larger. Two peaks can be seen for each curve. For the three greatest heights from the ground, the twin peaks seem approximately the same size. However, for the smallest height, $h_r/c=0.067$, the lower peak seems significantly larger than the upper peak. These are attributed to the vortex shedding. At the smallest height of $h_r/c=0.067$, the increased size of the lower peak is accounted for by the separating suction surface boundary layer. Similar twin peaks in the *uu* distribution were found in work (Koss *et al*., 1993), using LDA results in the near-wake region of a divergent trailing edge (DTE) aerofoil. As the ground is approached, the magnitude of the fluctuating velocity increases for all cases apart from the closest height from the ground. Although not illustrated here, results at $h_r/c=0.090$ show a higher peak *uu* value than that at $h_r/c=0.067$. The results taken close to the ground in the region between the ground plane and the constant velocity accelerated fluid region suggest that the ground flow region, including the velocity deficit area is turbulent in nature.

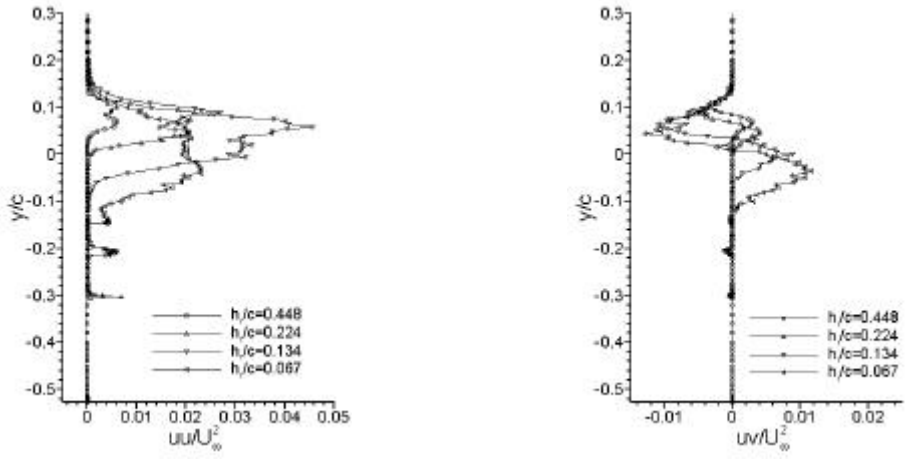

a) *b)*

Fig. 12. Mean flow turbulent velocity wake profiles at x/c=1.5, (a) uu/U¥ (b) uv/U¥

3.4 Implications of Results

Aerodynamic interactions between wake from the front wing and the downstream devices are critical for the performance of the overall car. For example, the wake from the front wing can be ingested into the sidepods and severely effect the efficiency of the radiators used for cooling of the mechanical devices. The flow to the undertray, leading to the diffuser and the rear wing is also significantly effected by the front wing wake.

The results show that, at a large height from the ground, a small wake results with relatively low levels of turbulence. This is desirable from the point of view of the downstream devices. The downforce generated at this height from the ground, unfortunately, is significantly lower than that which could be generated in closer proximity to the ground. However, the large wake which features at small ground heights results in higher levels of turbulence and more mixing in the wake. This effective high freestream turbulence significantly effects the performance of the downstream aerodynamic devices.

4. CONCLUSION

The instantaneous and time-averaged flow properties of the wake region of a wing in ground effect with a finite trailing edge have been identified. The following conclusions can be drawn:

- At a large ground height, discrete, alternate vortex shedding was identified from instantaneous PIV flow snapshots. The mean flow shows a small turbulent wake, growing, and moving upwards as it travels downstream.
- As the ground height is reduced, boundary layer separation occurs on the suction surface. The instability of the shear layer produces vortices. The amplification of the instability waves also leads to non-linear roll-up of the shear layer: i.e., large vortices. The shear layer experiences a couple motion of flapping in the transverse direction and vortex convection in the streamwise direction. The size of the turbulent wake grows, especially on the suction side, due to the boundary layer separation at that side. This has a turning effect on the wake, such that as the wake develops, it comes closer to the ground.

ACKNOWLEDGEMENT

Jonathan Zerihan wishes to thank the EPSRC for providing a Ph.D. studentship. The authors would like to thank Willem Toet of British American Racing for his support and. Technical assistance was given by the Tyrrell Racing Organisation and British American Racing. The efforts of Geoff Thomas in construction of the model are greatly appreciated.

REFERENCES

Benedict, L. and Gould, R., "Towards better uncertainty estimates for turbulence statistics", Experimental Thermal and Fluid Science, Vol. 22, No. 2, pp. 129-136

Burgin, K., Adey, P. and Beatham, J., "Wind tunnel tests on road vehicle models using a moving belt simulation of ground effect", Journal of Wind Engineering and Industrial Aerodynamics, Vol. 22, pp. 227-236.

Jeffrey, D., Zhang, X. and Hurst, D., "Aerodynamics of Gurney flaps on a single-element high-lift wing", Journal of Aircraft, Vol. 37, No. 2, March-April 2000, pp. 295-302.

Khorrami, M., Berkman, M., Choudhari, M., Singer, B., Lokhard, D. and Brentner, K., "Unsteady flow computations of a slat with a blunt trailing edge", AIAA Paper 99-1805, 1999.

Koss, D., Bauminger, S., Shepshelovich, M., Seifert, A. and Wygnanski, I., "Pilot test of a low Reynolds number DTE airfoil", AIAA Paper 93-0643, 1993.

Moffat, R., "Contributions to the theory of single-sample uncertainty analysis", Transactions of the ASME: Journal of Fluids Engineering, Vol.104, June 1982, pp. 250-260.

Pailhas, G., Sauvage, P., Touvet, Y. and Coustols, E., "Flowfield in the vicinity of a thick cambered trailing edge," 9th International Symposium on Applications of Laser Techniques to Fluid Mechanics, Lisbon, Portugal, July 13-16, 1998.

Vassilopoulos, K. and Gai, S., "Unsteady pressures on a blunt trailing edge - end plate and boundary layer effects", AIAA Paper 98-0418, 1998.

Zerihan, J. and Zhang, X., "Aerodynamics of a single element wing in ground effect", AIAA Paper 2000-0650, AIAA 38th Aerospace Sciences Meeting, January 11-13, 2000.

Zhang, X and Zerihan, J., "Force enhancement of Gurney flaps on a wing in ground effect", AIAA Paper 2000-2241, Fluids 2000, June 19-22, 2000.

h_r/c	x/c	u_{min}/U_{∞}	y at u_{min}	y at d_{top}	y at d_{bottom}	d
0.448	1.5	0.81	0.08	0.13	0.04	**0.09**
	2.0	0.90	0.10	0.16	0.04	**0.12**
	3.0	0.93	0.13	0.22	0.06	**0.16**
0.313	1.5	0.81	0.08	0.13	0.04	**0.09**
	2.0	0.89	0.09	0.16	0.04	**0.13**
	3.0	0.93	0.14	0.22	0.04	**0.18**
0.224	1.5	0.79	0.07	0.13	0.01	**0.11**
	2.0	0.88	0.08	0.16	0.01	**0.15**
	3.0	0.93	0.12	0.20	0.01	**0.19**
0.179	1.5	0.78	0.05	0.12	-0.02	**0.14**
	2.0	0.88	0.06	0.15	-0.03	**0.18**
	3.0	0.91	0.07	0.19	-0.03	**0.22**
0.134	1.5	0.77	0.04	0.12	-0.05	**0.17**
	2.0	0.85	0.04	0.14	-0.07	**0.21**
	3.0	0.91	0.05	0.19	-0.08	**0.27**
0.112	1.5	0.73	0.04	0.13	-0.07	**0.20**
	2.0	0.85	0.04	0.16	-0.08	**0.24**
	3.0	0.91	0.06	0.20	-0.10	**0.30**
0.090	1.5	0.72	0.02	0.12	-0.10	**0.22**
	2.0	0.84	0.02	0.16	-0.11	**0.27**
	3.0	0.90	0.01	0.19	-0.12	**0.31**
0.067	1.5	0.66	0.00	0.13	-0.11	**0.23**
	2.0	0.77	-0.01	0.17	-0.10	**0.27**

Table 1. Wake information; LDA results